https://doi.org/10.5194/cp-2024-8
Preprint. Discussion started: 26 February 2024

Climate of the Past
Discussions

South Asian summer monsoon enhanced by the uplift of Iranian Plateau in Middle Miocene

Meng Zuo[1,2], Yong Sun[3], Yan Zhao[3*], Gilles Ramstein[4], Lin Ding[3], Tianjun Zhou[1]

1 LASG, Institute of Atmospheric Physics, Chinese Academy of Sciences, Beijing, China

2 State Key Laboratory of Severe Weather and Institute of Tibetan Plateau Meteorology, Chinese Academy of Meteorological Sciences, Beijing, China

3 Key Laboratory of Continental Collision and Plateau Uplift, Institute of Tibetan Plateau Research, and Center for Excellence in Tibetan Plateau Earth Sciences, Chinese Academy of Sciences, Beijing 100101, China

4 Laboratoire des Sciences du Climat et de l'environnement, CNRS-CEA-UVSQ, 91191 Gif-sur-Yvette, France

Correspondence to yan zhao: yan.zhao@itpcas.ac.cn

https://doi.org/10.5194/cp-2024-8
Preprint. Discussion started: 26 February 2024

Climate of the Past Discussions

ABSTRACT

The South Asian summer monsoon (SASM) significantly intensified during the Middle Miocene (17-12 Ma), but the driver to this change remains an open question. The uplift of the Himalaya (HM) and Iranian Plateau (IP), and global CO_2 variation are prominent factors among suggested drivers. Particularly the impact of high CO_2 on the Miocene SASM is little studied despite a large range of reconstructed CO_2 values around this period. Here we investigate their effects on the SASM using the fully coupled Ocean-Atmosphere Global Climate Model CESM1.2 through a series of 12 sensitivity experiments. Our simulations show that the IP uplift plays a dominant role in the intensification of the SASM, mainly in the region around northwestern India. The effect of the HM uplift is confined to the range of the HM and its vicinity, producing orographic precipitation change. The topography forcing overall out-competes CO_2 variation in driving the intensification of the SASM. In the case of extremely strong CO_2 variation, the effects of the two factors are comparable in the core SASM region while in the western region, the topographic forcing is still the dominant driver. A thermodynamical process is proposed to link the uplift of the IP and enhanced SASM through latent heating release. Compared with reconstructions, the response of SASM to the IP uplift is in good agreement with observed precipitation and wind while the effects of the HM uplift and CO_2 variation are inadequate to interpret the proxies.

Keywords: South Asian summer monsoon, Middle Miocene, topographic change, CO_2 variation, thermal heating effect

https://doi.org/10.5194/cp-2024-8
Preprint. Discussion started: 26 February 2024

1. Introduction

The Middle Miocene (17-12 Ma) was a period characterized by major climatic, tectonic, CO_2 and environmental changes (Steinthorsdottir et al., 2021). Increasing evidences indicate that the South Asian summer monsoon (SASM) was remarkably intensified in the Middle Miocene (Clift et al., 2008; Clift and Webb, 2019; Gupta et al., 2015; Zhuang et al., 2017; Bialik et al., 2020; Bhatia et al., 2021; Vogeli et al., 2017) although its inception was no later than the Early Miocene (Ali et al. 2021, Licht, 2014; Farnsworth et al., 2019). However, the driving factor of its evolution remains an issue of great debate. Besides the effect of geographic change (Ramstein et al., 1997; Fluteau et al., 1999; Farnsworth et al., 2019; Thomason et al., 2021; Tardif et al., 2020, 2023; Sarr et al., 2022), the growth of the Himalaya (HM)-Tibetan Plateau (TP; HM-TP) has traditionally been called for the SASM development (Zhuang et al., 2017; Cliff et al., 2008; Clift and Webb, 2019; Manabe and Terpstra, 1974; Kutzbach et al., 1989; Prell and Kutzbach, 1992; Ramstein et al., 1997; An et al., 2001; Kitoh, 2002; Chakraborty et al., 2006; Wu et al., 2012; Tada et al., 2016; Tarif et al., 2020, 2023).

The HM, which has long been regarded as the "southern TP" (Spicer, 2017), receives particular attention (Boos and Kuang, 2010; Wu et al., 2012; Zhang et al., 2015). Recent geological evidences (Liu et al., 2016; Ding et al., 2017, 2022) suggest that, in contrast to previous studies, the HM had risen to a height of 2.3 ± 0.9 km by the earliest Miocene, reaching approximately 4 km by 19 Ma. From 15 Ma onwards, the HM projected significantly above the average elevation of the plateau. This elevation was notably higher than the TP, which had reached its modern height before the Miocene (Wang et al., 2014). The coincidence of the rapid HM uplift and the intensification of SASM appears to support the hypothesis that the evolution of the SASM is predominantly driven by the formation of HM-TP.

However, this traditional view is challenged by many modeling studies which emphasize the importance of peripheral mountain ranges (Chakraborty et al., 2006; Tardif et al., 2020, 2023; Sarr et al., 2022; Liu et al., 2017; Tang et al., 2013; Chen et al., 2014; Acosta and Huber, 2020). Notably, the Iranian Plateau (IP), which also experienced uplift during the same period as the Miocene SASM enhancement around 15-12 Ma, is regarded as a critical factor (McQuarrie et al., 2003; Mouthereau, 2011; Ballato et al., 2017; Bialik et al., 2020). Therefore, the contribution of the IP and HM uplift to intensified SASM during the Middle Miocene remains unclear.

Various mechanisms were proposed to explain the linkage between the uplift of the IP and HM and the intensification of SASM rainfall, including the mechanical blocking effect (Tang et al., 2013), topographic thermal forcing (Chen et al., 2014; Wu et al., 2012; Liu et al., 2017), and the role of gatekeeper to insulate the pool of high-enthalpy air in northern India from westerly advection of cool and dry air (Acosta and Huber, 2020). However, most of these modeling studies examined the effects of IP and HM uplift based on Atmospheric general circulation model with modern geographies (Liu et al., 2017; Zhang et al., 2015; Tang et al., 2013; Acosta and Huber, 2020), which may result in two key issues: 1) neglecting the air-sea interaction process (Kitoh, 2002; Su et al., 2018; Wang et al., 2019); 2) a misleading interpretation for past changes due to the critical role of land-sea distribution in shaping the paleoclimate features (Tardif et al., 2023; Ramstein et al., 1997). Therefore, it is worthy to revisit the response of the SASM to the IP and HM uplift under Miocene boundary conditions with a fully coupled Ocean-Atmosphere Global Climate Model (OAGCM) and investigate the underlying physical processes, which have been rarely studied before (Sarr et al., 2022; Tardif et al., 2022, 2023).

The SASM is sensitive to changes in CO_2 concentration (Thomason et al., 2021). The effect of pCO_2 variation is overall estimated to be less than that of geography and/or topography (Farnsworth et al., 2019; Thomason et al., 2021; Tardif et al., 2023), however, during the mid-to-late Miocene, its contribution to rainfall change is comparable to that of orographic uplift even when the pCO_2 is set from 280 ppm to 560 ppm (Thomason et al., 2021). Proxy records indicate the early to middle Miocene was a warming period, which is known as the Middle Miocene Climatic Optimum (~17-14 Ma), followed by a late Miocene cooling (Steinthorsdottir et al., 2021b). There is large uncertainty in estimated pCO_2 variation in the Middle Miocene, with a wide range of reconstructed values from ~180 ppmv to ~600 ppmv (Foster and Rohling, 2013; Pagani et al., 1999; Steinthorsdottir et al., 2021; CenCO_2PIP, 2023, and reference herein), even to more than 1000 ppmv (Rae et al., 2021) during the Middle Miocene Climatic Optimum. Therefore, it is necessary to re-examine the effect of pCO_2 forcing on SASM rainfall based on the possible range of pCO_2 variation.

In this study, a fully coupled OAGCM is employed to explore the impact of IP and HM uplift and the CO_2 variation on the SASM. The topographic sensitivity experiments are placed into the context of the current understanding of the regional tectonic and geographic settings. A set of CO_2 sensitivity experiments with a range of values from 280 to 1000 ppmv is performed based on the Middle Miocene geography. The model configuration, Middle Miocene boundary condition and experimental design are described in Section 2. In Section 3, we show the SASM response to IP and HM uplift, and the effect of CO_2 forcing. The mechanisms responsible for the monsoonal precipitation change are examined in Section 4. The implication of our results to the evolution of the SASM in the Middle Miocene is discussed in Section 5 before giving conclusions in Section 6.

2. Data and Methods

2.1. Climate model

The model used in this study is the Community Earth System Model (CESM), Version 1.2.1 of the National Center for Atmospheric Research. It includes the Community Atmosphere Model (CAM4) (Neale et al., 2013), the Community Land Model (CLM4; Hunke and Lipscomb, 2010), the Parallel Ocean Program (POP2; Smith et al., 2010), the Community Ice Sheet Model and the Community Ice code (Glimmer-CICE4). CLM4 incorporates a dynamic vegetation module (Lawrence et al., 2011) which is switched off in this study. The horizontal resolution used is 1.9°(latitude) × 2.5° (longitude) for CAM4 with 26 vertical levels and CLM4 has identical horizontal resolution. CESM has been extensively used for modern and the tectonic climate studies (Chen et al., 2014; Goldner et al., 2014; Frigola et al., 2018). In general, this model simulates modern surface temperature distributions and equator-to-pole temperature gradients well (Gent et al., 2011), although biases exist (Neale et al., 2013). However, it strongly overestimates the Miocene meridional temperature gradient compared to reconstructions, a thorny problem for Miocene modeling practice (Burls et al., 2021; Steinthorsdottir et al., 2021) mainly caused by the inability of climate models to reproduce polar amplified warmth (Krapp and Jungclaus, 2011; Herold et al., 2011; Goldner et al., 2014; Burls et al., 2021). Nevertheless, the temperature biases in low latitudes are small, generally within 1°C (Burls et al., 2021).

2.2. Boundary conditions

Our Miocene experiments are configured with geography, topography, bathymetry and vegetation cover from Frigola et al. (2018, henceforth F18), which provides boundary conditions for modeling studies with a focus on the Middle Miocene. According to F18, the most prominent geographic differences between the Middle Miocene and present day are the opening of the Tethys, Indonesian and Panama seaways, the closure of the Bering Strait and lower elevations of most of the highest regions of the globe. For instance, the African topographies were reduced to 25% of its current elevation (Figs. 1a and b).

The topography of the Tibetan Plateau in F18 is set to its estimated Early to Middle Miocene elevation. The southern and central plateau reached a near modern elevation, the

https://doi.org/10.5194/cp-2024-8
Preprint. Discussion started: 26 February 2024

northern plateau is set to 3-4 km but its northward extend is reduced to reflect the rapid uplift occurring in Pliocene (Harris, 2006, and the references therein). The HM reached to 60-80% of its present height. As for the IP, here we lumped together all the mountain ranges west of the Himalayan, including the Hindu Kush region and Pamir as the IP. The northern part of the IP reached a near modern elevation as 1000-2000 m, but its southern part was lower than 1000 m.

The Miocene vegetation is prescribed as that in F18, which is a global gridded distribution (Figure S1 in Supplementary Materials (SM)) merging previous reconstructions (See F18 for more details). During the Miocene, vegetation types associated with lower latitudes today encroached on higher latitudes. There was reduced presence of ice compared to modern conditions, and ice-free regions were covered by tundra in Antarctica while cold mixed forests spread over Greenland.

2.3. Experimental design

We first perform two simulations: the pre-industrial (piControl) and the Middle Miocene (MMIO) simulation, which differ in their applied geography (Figs. 1a and b), bathymetry, vegetation cover and the CO_2 concentrations while the solar constant, orbital configuration and the concentrations of other greenhouse gases are kept at their modern values. The CO_2 concentration is set to 280 ppmv in the piControl (Eyring et al., 2016) and 400 ppmv in the MMIO following the setting of F18. The choice of 400 ppmv is somewhat low but within the range of published estimates (see details in F18 and Burls et al., 2021). Both simulations are integrated to reach quasi-equilibrium, particularly the MMIO experiment is integrated over 3000 years. The difference between MMIO and piControl provides the background information of the simulated changes in the SASM between the two periods.

Based on the MMIO simulation, we run a set of experiments with altered orography in the HM and the IP. We examine the joint effects of the HM and IP on the SASM assuming the HM and the IP rise simultaneously from flat (0%) to 100% of their reference height (Figs. 1c and d). The reference height is the modern altitude for the HM and the reconstructed Miocene altitude for the IP. The experiments are referred as IP0HM0 and IP100HM100, respectively. To further separate the climatic effect of the IP and HM uplift, we conduct another two experiments: IP100HM0 and IP0HM100. In the former (latter) experiment, the HM (IP) is absent while the IP (HM) reaches its reference height (Figs.1e and f). Combined with the experiments of IP0HM0 and IP100HM100, the effect of elevated IP and HM is estimated (see section 3.2). To further reveal the impact of the IP uplift on the SASM evolution, two other experiments are conducted: IP50HM0 and IP50HM100, indicating that the IP is reduced by half of its Miocene height while the HM is absent and fully uplifted, respectively.

To clarify the relative role of pCO_2 forcing on SASM rainfall in the Middle Miocene, we also run a set of CO_2 sensitivity experiments with the pCO_2 setting to 280, 560, 800 and 1000 ppmv, referred to as MMIO280, MMIO560, MMIO800 and MMIO1000, respectively. The high values as 800 and 1000 ppm are chosen because new reconstructions of pCO_2 are generally correspond to 3 times the pre-industrial levels (Rae et al., 2021). These experiments share the same boundary conditions as the MMIO simulation, differing only in CO_2 concentration.

The simulations considered in our study are listed in Table 1. The sensitivity experiments are integrated from the MMIO equilibrium state for another 200 (500) years for the topography (CO_2) sensitivity experiments to reach quasi-equilibrium. The final 50 years of these simulations are used for analysis.

2.4. Monsoon indices

The following indices are defined to illustrate features of the SASM changes.

(1) All Indian rainfall (AIR): regional mean precipitation over the land points within the domain of 7-30°N, 65-95°E.

(2) Webster-Yang Index (WYI; Webster and Yang, et al., 1992): meridional wind stress shear between 850 hPa and 200 hPa averaged over 40-110°E, 0-20°N during June-August.

(3) Somali jet strength (SMJ; Sarr at al., 2022): Maximum intensity of the Somali jet over the Arabian Sea (averaged over 30-60°E, 0-20°N) during June-August.

2.5. Moisture budget analysis

Moisture budget analysis (MDA) can decompose the precipitation change into changes in evaporation and moisture advection (Chou et al. 2009). It relates the net precipitation (precipitation minus evaporation; P - E) to the vertically integrated moisture flux convergence (Chou et al., 2009). More details about MDA are given in SM 2. This method has been widely applied to paleoclimate studies in recent years, such as distinguishing the physical processes involved in precipitation changes in Mid-Holocene (Sun et al., 2023). Here, we apply MDA to reveal the physical processes related to SASM precipitation responses to the uplift of IP-HM and to pCO_2 change.

https://doi.org/10.5194/cp-2024-8
Preprint. Discussion started: 26 February 2024

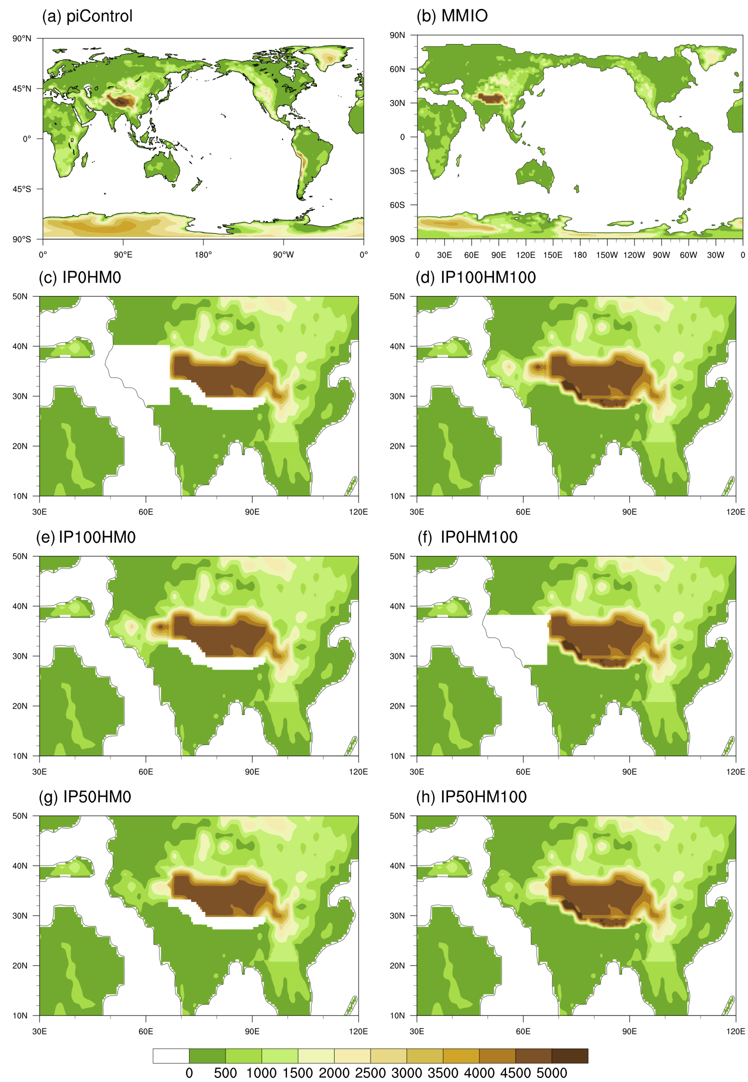

Figure 1. Topography of (a) piControl, (b) MMIO and orographic sensitivity experiments, including (c) IP0HM0, (d) IP100HM100, (e) IP100HM0 and (f) IP0HM100, (g) IP50HM0, (h) IP50HM100 (The maps are plotted at 0.5°x0.5° resolution. The same maps but at 1.9°x2.5° resolution are provided in the SM as Fig. S2)

https://doi.org/10.5194/cp-2024-8
Preprint. Discussion started: 26 February 2024

3. Results

3.1. Climatology of the SASM in the present day and Middle Miocene

The CESM1.2 is one of the best models in simulating the present-day SASM (Anand et al., 2018; Jin et al., 2020). The CESM1.2 reproduced the broad features of the SASM system including the onshore flows and strong monsoonal precipitation when compared to the observational datasets including GPCP (precipitation) and ERA5 (circulation) (Huffman et al., 2009; Hersbach et al. 2020). The maximum centers of precipitation are reasonably captured over the southern slope of the HM, the East Arabian Sea and Bay of Bengal despite biases in intensity and extensions (Figs. 2a, b), which is largely due to the coarse spatial resolution (Acosta and Huber, 2017**;** Anand et al., 2018; Botsyun et al., 2022a, b; Boos and Hurley, 2012). Thus, we focus on the large-scale circulations and treat the local features with caution. The regional mean precipitation, as measured by the AIR, is 7.7 mm day^{-1} in GPCP and 8.7 mm day^{-1} in the piControl experiment. The positive bias reflects an overestimation of precipitation in the Western Ghats and at the HM foothills.

Compared with the piControl experiment, the MMIO simulation displays apparent adjustment of the JJA mean low-level circulation. The westerlies pass Africa into the Indian region and a cyclonic circulation develops over the Arabian Sea, the cross-equatorial flow weakens and displaces southward (Fig. 2c). There is considerable enhancement of monsoonal precipitation in South Asia but not limited there (Fig. 2c). AIR in MMIO simulation is 10.4 mm day^{-1}, which is ~20% higher than that in piControl experiment.

The wetter Miocene climate is also reflected by the widespread Africa-Asian monsoon, which was suggested by previous modeling studies (Herold and Huber, 2011; Zhang et al., 2015). Here a monsoon-like climate is defined as local summer-minus-winter precipitation exceeding 2 mm day^{-1} and the local summer precipitation exceeding 55% of the annual total (Wang and Ding, 2008). This monsoon index is determined by the intensity of summer monsoonal precipitation in the region of the South Asian Monsoon (SAM). Compared with present day, the domain of the SAM extends westward both in land and over the Arabian Sea where it nearly connects the African monsoon (Fig. 3c), a feature also presented in the study of Fluteau et al. (1999). The distribution of the simulated SAM is generally consistent with the proxies (Table 2), confirming the wide existence of SAM in the Middle Miocene in terms of rainfall seasonality.

https://doi.org/10.5194/cp-2024-8
Preprint. Discussion started: 26 February 2024

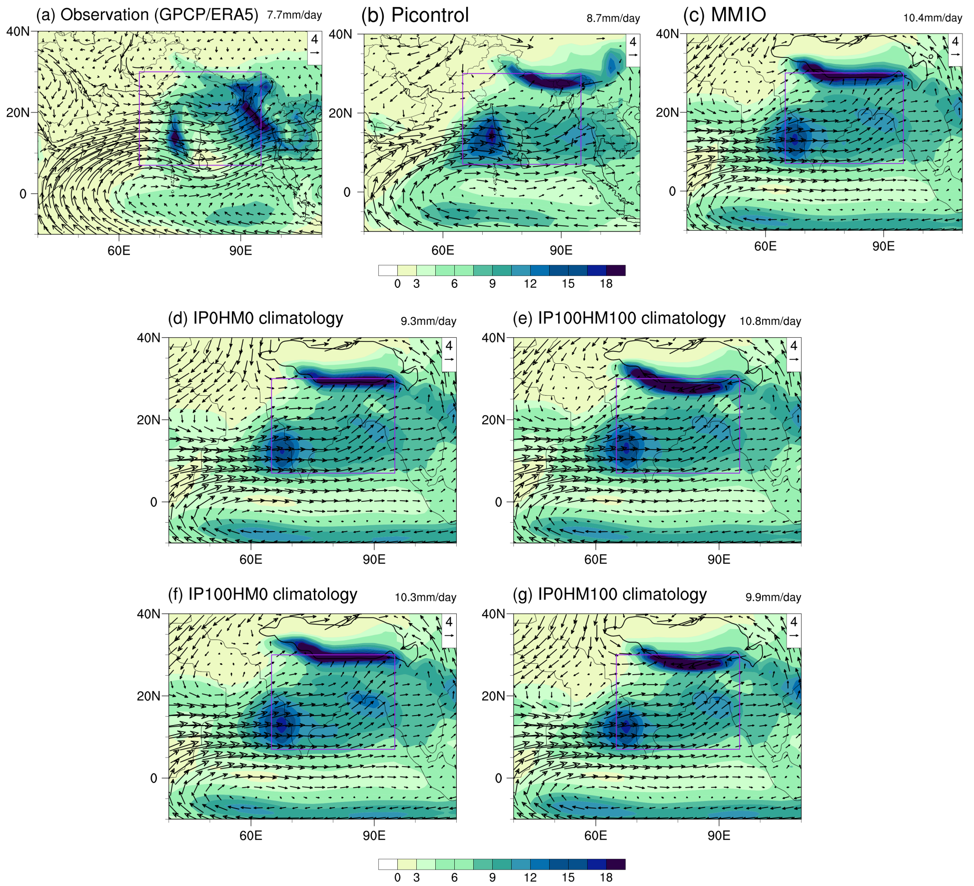

Figure 2. Climatology of JJA (June-July-August) seasonal mean South Asia summer monsoon (SASM) precipitation (mm day^{-1}) and 850 hPa winds (vectors, m s^{-1}) from (a) observation precipitation from GPCP and circulation from ERA5), (b) Preindustrial control experiment and (c) MMIO experiment. (d) IP0HM0, (e) IP100HM100, (f) IP100HM0, (g) IP0HM100. Climatology is the average over 1979-2005 for the observation. As for the piControl and MMIO experiment, we select the last 50 and 100 years of simulation, respectively. All Indian rainfall (AIR) is shown at the top-right of each panel. AIR indicates precipitation over the land points within the purple square in each panel (7-30°N, 65-95°E). The black contour in panel (c)-(g) indicates the altitude of 2500 m.

https://doi.org/10.5194/cp-2024-8
Preprint. Discussion started: 26 February 2024

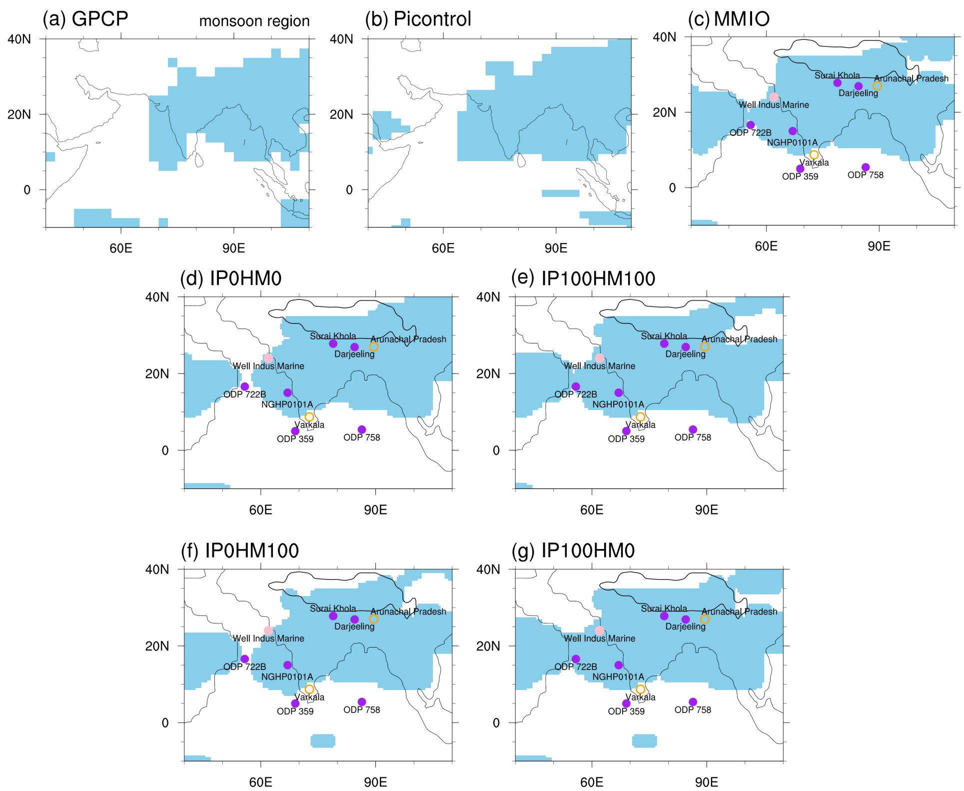

Figure 3. The monsoon domains (blue shading) in (a) GPCP, (b) piControl experiment, (c) MMIO experiment, (d) IP0HM0, (e) IP100HM100, (f) IP0HM100 and (g) IP100HM0 experiments, which are defined by the regions where local summer-minus-winter precipitation exceeds 2 mm day^{-1} and the local summer precipitation exceeds 55% of the annual total. Dots in (c-g) represent reconstructions near the SASM region, purple solid dots denote enhanced SASM, orange circles denote no significant change and pink solid dots denote weakened SASM from middle to late Miocene. The black contour in panel (c)-(g) indicates the altitude of 2500 m.

3.2. The effect of the HM and IP uplift

We first examine the effect of the joint uplift of the HM and IP (hereafter referred to as IP-HM). With the uplift of the IP-HM (Fig. 4a), a prominent cyclonic anomaly is built to the west of the IP with the intensified southwesterlies from Africa via the Arabian Sea into the northwestern India. This anomaly regarded as the deepening of thermal low is also shown in

https://doi.org/10.5194/cp-2024-8
Preprint. Discussion started: 26 February 2024

Climate of the Past Discussions

previous study (Sarr et al., 2022). Increased precipitation is found along the eastern flank of the cyclonic anomaly to the slopes of the western HM and northeastern IP. In the eastern part of the monsoon region, the enhanced precipitation occurs mainly along the southern edge of the HM while the leeward side features a remarkably decreased precipitation, indicating the rain shadow effect.

Corresponding to the summer precipitation change in response to IP-HM uplift, the domain of the SASM expands westward over the Arabian Sea and the Indian subcontinent (Figs. 3d-e). The western extension over land is about 65°E in the IP0HM0 experiment and reaches 60°E in the IP100HM100 experiment, indicating that the change of the SASM is significant in the northwest of the Indian subcontinent. Interestingly, monsoonal signal exists in the IP0HM0 experiment, an analogue to the "early Miocene", indicating that proto-monsoon exists by having TP only, which is also found in previous studies (Sarr et al., 2022). At the site of ODP 722B, monsoonal signal is absent in IPHM0 (Fig.3d), but present in IP100HM80 (MMIO, Fig. 3c) and IP100HM0 (Fig. 3e) when the IP-HM is uplifted.

We further separate the effect of the IP and HM uplift. The climate response to IP uplift (IP100-IP0) is estimated as ((IP100HM0-IP0HM0)+(IP100HM100-IP0HM100))/2. Similarly, the effect of HM uplift HM100-HM0 is estimated as ((IP0HM100-IP0HM0)+(IP100HM100-IP100HM0))/2. The changes in precipitation and low-level circulation much resemble that attributing to the IP-HM uplift (Fig. 4a), indicating that by itself, the IP can sustain major parts of the precipitation changes except over the central-eastern HM. The easterly anomaly across the Indian subcontinent indicates that the westerly is blocked by elevated IP from north India, facilitating moisture convergence and rainfall increase over the northern Indian continent. As a result, the regional mean precipitation increases by 1.1 and 2.0 mm/day over the core and western regions (15-35°N, 50-75°E), respectively.

In contrast to the widespread effect of the IP on the SASM, the HM uplift only has a local effect (Fig. 4c), which is mostly confined to the HM and its close vicinity, and the change in low level circulation is noisy and weak. The precipitation strongly increases along the southern slope of the HM and dramatically decreases on its leeward side, resembling the changes in precipitation in the eastern region caused by the IP-HM uplift. As a result, there is little change in the regional mean precipitation over the core and eastern regions (15-35°N, 75-95°E).

https://doi.org/10.5194/cp-2024-8
Preprint. Discussion started: 26 February 2024

In summary, the joint influences of the IP-HM uplift on the SASM are the superimposed effect of the IP and HM. In the western region, i.e., from the Arabian Sea to the northwestern India and Pakistan, the IP plays a dominant role while in the eastern region, i.e., the east part of South Asia, the changes in the SASM mainly attribute to the HM uplift. And the western extension of the SASM domain over the Arabian Sea and the Indian subcontinent is mainly caused by the uplift of IP rather than HM (Figs. 3f-g).

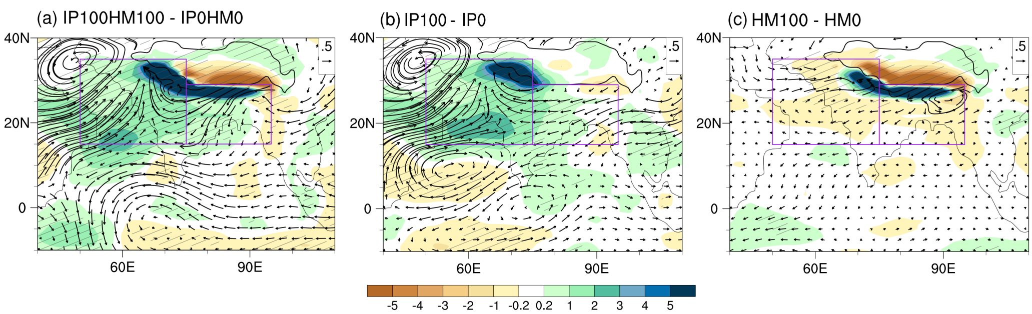

Figure 4. Precipitation (shaded, mm day^{-1}) and 850hPa wind differences between (a) IP100HM100 and IP0HM0 experiments; (b) IP100 and IP0 experiments; (c) HM100 and HM0 experiments. Here IP100-IP0=((IP100HM0-IP0HM0)+(IP100HM100-IP0HM100))/2, HM100-HM0=((IP0HM100-IP0HM0)+(IP100HM100-IP100HM0))/2. The black contour in each panel indicates the altitude of 2500 m. Purple boxes represent west (15-35°N, 50-75°E) and east (15-29°N, 75-95°E) parts of the South Asian monsoon region. Slashes indicate values >95% confidence level based on the *Student's t* test.

3.3. The effects of the pCO_2 forcing vs topographic forcing

To illustrate the effect of pCO2 forcing on SASM during the MMIO, we show the climatology of the SASM at low and high levels of CO_2 concentration based on MMIO28 and MMIO1000 experiments, respectively (Fig.5). The spatial circulation patterns in these two experiments are similar to that in the MMIO but the magnitudes change significantly (Fig.5a and b, Fig.2c). With the increase of pCO_2, the meridional cross-equatorial flow slightly strengthens along the East Africa coast until 15°N but weakens to its west (Fig. 5c, d), leading to little change in the regional mean strength of this flow over the Arabian Sea. Meanwhile, precipitation enhances along the band of 15-25°N but decreases to its south, indicating a northward shift of the tropical rainfall belt. As the pCO_2 rises from 280 ppm to 400 ppm, and subsequently to 1000 ppm, the AIR index correspondingly increases by 0.5 mm day^{-1} and 1.2

mm day^{-1}, respectively. MBA (SM2) further reveals that the increased monsoonal precipitation is primarily induced by enhanced thermodynamic conditions due to atmospheric warming, while the contribution from the change in large-scale monsoon circulation plays a secondary role (SM Fig S5c and d). For instance, the precipitation change between MMIO1000 and MMIO in the core SASM region is 1.2mm/day, of which 0.6 is from the thermodynamical processes related to changes in moisture and 0.25 mm/day from the dynamical processes related to circulation change. Similar conclusion is also reported in projecting future climate change facing the rising CO_2 (Endo and Kitoh, 2014).

To compare the effect of pCO_2 forcing versus topographic forcing on the SASM, we examine the changes of precipitation and low-level circulations between MMIO1000 and IP0HM0 experiments (Fig. 5e), which actually reflects the combined effects of the CO_2 forcing (MMIO1000-MMIO) and IP-HM uplift (MMIO-IP0HM0). It is clear that the SASM changes in Fig. 5e bear the features of Fig. 5d and Fig. 4a: precipitation enhancing along the band of 15-25°N and reducing to its south in response to increased pCO_2 and a prominent cyclonic anomaly built to the west of the IP in response to the IP-HM uplift. Moisture budget analysis further reveals that the enhanced precipitation of 3.2 mm day^{-1} in the west part of the SAM region is equally attributed to the vertical and horizontal moisture advection of 2.3 mm day^{-1} (Fig. 6). The moisture advection by anomalous meridional winds is the dominant contribution term, which is actually the response to the IP uplift as we see in next section.

We further examine the impacts of pCO_2 forcing and topographic forcing in terms of WYI, SMJ, AIR (Sect. 2.4) and the mean precipitation over the western part of the SASM region (Fig.7). Under the topographic forcing, WYI exhibits small changes, with the exception of a relatively lower value in the IP0HM100 experiment. Concurrently, both precipitation and low-level circulation indices increase in response to the IP uplift, indicating a quasi-circulation-rainfall coupling relationship. With the increasing of pCO_2 forcing, there is a noticeable decrease in WYI, whereas AIR and precipitation in the western SAM region increase significantly, indicating a decoupling relationship between large-scale circulation and monsoonal rainfall. The cross-equator flow at lower level (Somali Jet) is insensitive to pCO_2 change as already shown in Fig.5.

The maximum difference of each index across the set of pCO_2 or topographic sensitivity experiments is defined as the effect of each driver. In terms of WYI (Fig. 7a), the effect of pCO_2 forcing is ~150% greater than that of IP-HM forcing, with values of 2.5 m s^{-1} vs 1.0 m s^{-1}.

https://doi.org/10.5194/cp-2024-8
Preprint. Discussion started: 26 February 2024

According to the AIR, the influence of pCO_2 forcing is ~1.5 mm day^{-1}, which is comparable to that of IP-HM forcing (~1.5 mm day^{-1}), but is larger than the individual contributions of IP forcing (~1.0 mm day^{-1}) and HM forcing (~0.5 mm day^{-1}). In the western region, the effect of pCO_2 forcing is about 75% compared to that of IP forcing (~1.5 vs ~2.0 mm day^{-1}). In summary, pCO_2 forcing is the dominant driver for large-scale monsoon circulation, while the uplift of the IP exerts a more significant effect on regional circulation and the associated precipitation.

We note that the SASM response to CO2 forcing in the Middle Miocene is very similar to that of projecting future climate change. For instance, increased SASM precipitation occurring with decreased WYI is also projected under abrupt quadrupling of CO_2 (Kong et al., 2022). The low-level monsoon circulations are projected to slightly weaken, consistent with the little change in the intensity of low-level cross-equator flow in our Miocene simulations (Fig.5 and 6). The similarity of the SASM response to CO_2 change suggests a similar physical mechanism operating in the two warm periods.

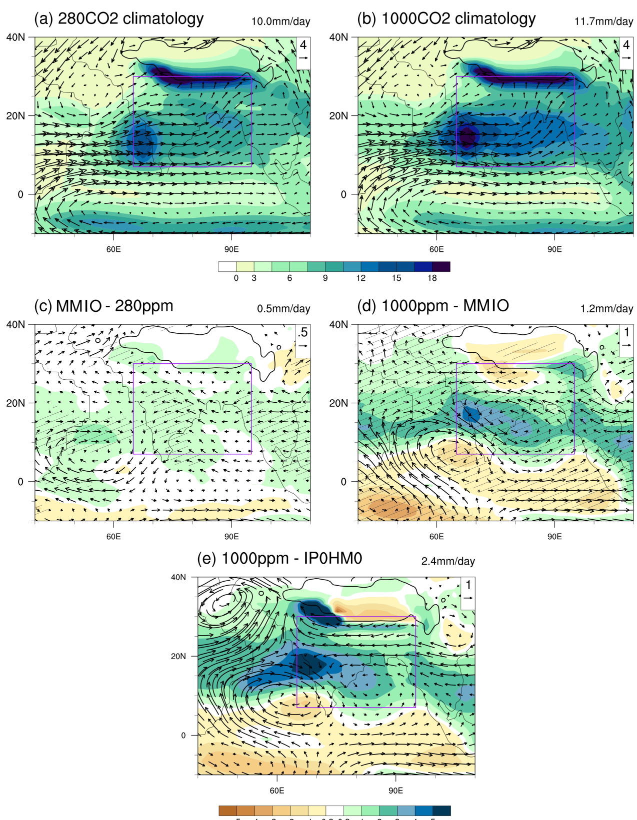

https://doi.org/10.5194/cp-2024-8
Preprint. Discussion started: 26 February 2024

Climate of the Past Discussions

Figure 5. Climatology of JJA (June-July-August) mean South Asia summer monsoon (SASM) precipitation (mm day^{-1}) and 850 hPa winds (vectors, m s^{-1}) from (a) MMIO_280 experiments and (b) MMIO_1000 experiments. Precipitation (shaded, mm day^{-1}) and 850hPa wind differences (vector, m s^{-1}) between (c) MMCO and MMCO_280 experiments; (d) MMCO_1000 and MMCO experiments; (e)MMIO_1000 and IP0HM0 experiments.

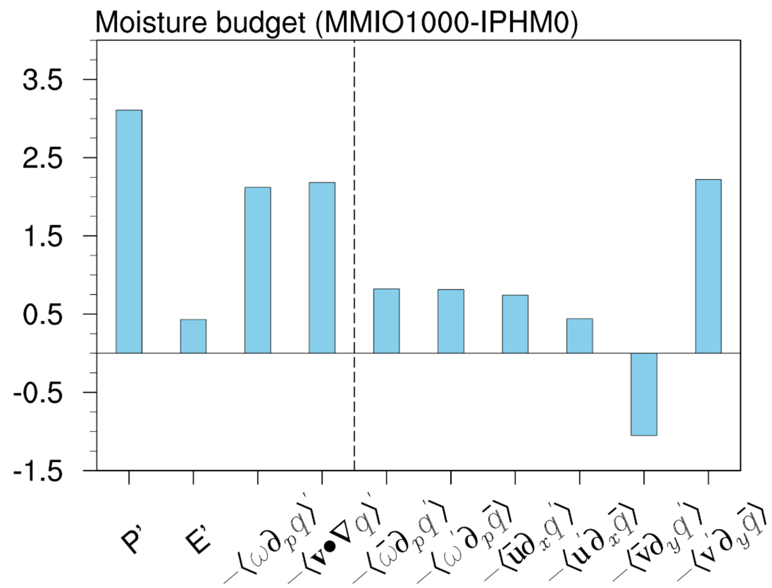

Figure 6. Moisture budget for regional mean precipitation differences (mm day^{-1}) over the west part (15-35°N, 50-75°E) of the South Asian monsoon region between MMIO1000ppm and IP0HM0 experiments.

https://doi.org/10.5194/cp-2024-8
Preprint. Discussion started: 26 February 2024

Climate of the Past
Discussions
Open Access
EGU

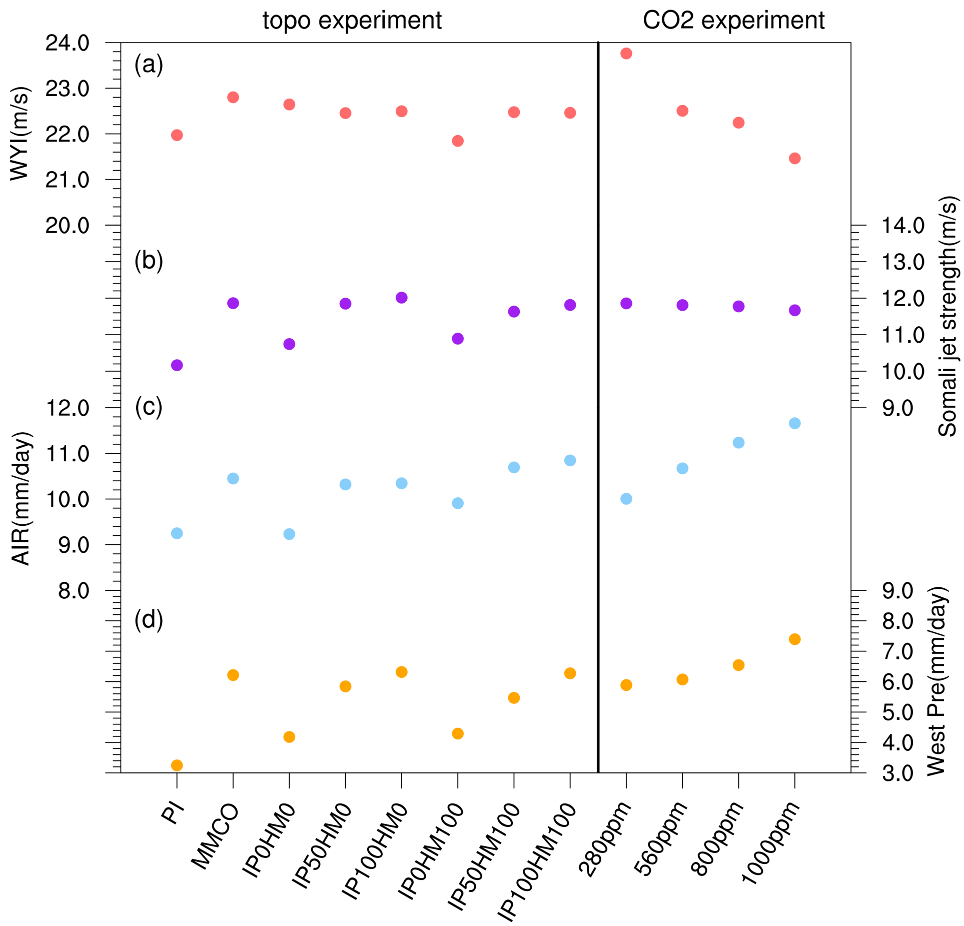

Figure 7. South Asian summer monsoon circulation and precipitation response in sensitivity experiments. Left, topography experiments. Right, CO_2 experiments. (a) Webster-Yang Index (meridional wind stress shear between 850 hPa and 200 hPa averaged over 40-110°E, 0-20°N during June-August). (b) Maximum intensity of the Somali jet over the Arabian Sea (averaged over 30-60°E, 0-20°N during June-August). (c) Regional mean precipitation over the land points within the domain (7-30°N, 65-95°E), named All indian rainfall (AIR). (d) Precipitation over the western part of South Asian summer monsoon region.

4. Mechanisms of the IP uplift on the SASM precipitation

To understand the mechanism of increased precipitation caused by IP uplift and HM uplift, we first use the moisture budget decomposition to identify the major moisture contributors. Here we provide the main analysis results (Fig.8), more details are seen in SM2. To focus our

https://doi.org/10.5194/cp-2024-8
Preprint. Discussion started: 26 February 2024

Climate of the Past
Discussions
Open Access

analyses on atmospheric dynamics, we neglect the contribution of evaporation, which is relatively small in our simulation despite the possibly important role for precipitation in the northwest India (Zhang et al., 2019). In response to IP uplift, the increased precipitation (2.0 mm day^{-1}) is largely attributed to the horizonal moisture advection (2.1 mm day^{-1}), in particular the moisture advection by anomalous meridional winds, while the vertical advection plays a secondary role (1.1 mm day^{-1}). In response to HM uplift, precipitation change (ca 1.2 mm day^{-1}) is mainly caused by the vertical moisture advection (0.9 mm day^{-1}) and is offset by the horizontal moisture advection (-0.4 mm day^{-1}). Its dominant contributor is a nonlinear term involving strong interaction between the vertical motion anomalies and moisture change (See SM2).

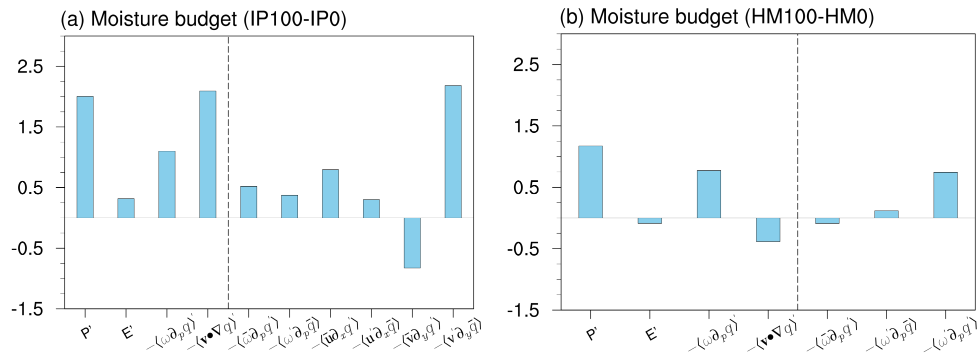

Figure 8. Moisture budget for regional mean precipitation differences (mm day^{-1}) over (a) the west part (15-35°N, 50-75°E) of the South Asian monsoon region between IP100 and IP0 experiments, (b) the east part (15-29°N, 75-95°E) of the South Asian monsoon region between HM100 and HM0 experiments.

We then examine the responses of the monsoon relevant variables to the uplifts of the IP and HM and the involved physical processes with focus on the effect of the IP. With IP uplift, the airs of high equivalent potential temperature (θ_e) at lower troposphere are accumulated in the IP and the surrounding region (Fig. 9a). The increased θ_e attributes to the enhancement of specific humidity (Fig. 9b) as moisture is advected by the anomalous southeasterly from north Africa via the Arabian Sea into the northwestern India and Pakistan (Fig. 9b), meanwhile it increases the convective instability. Triggered by surface sensible heating (Wu et al., 2012; ~~Medina et al., 2010~~), convection takes place. At 500hPa, the upward motion anomalies are found over the IP and along the HM (Fig. 9c), reflecting the lifting effect of the elevated topography. The height of the lifted condensation level (LCL) is significantly reduced over the

https://doi.org/10.5194/cp-2024-8
Preprint. Discussion started: 26 February 2024

IP and along the western edge of the HM (Fig. 9d), which is likely resulted from the elevated surface sensible heating (He, 2017). Reduced LCL facilitates the moist convection to occur, further warming the air parcels by the released latent heating. Consequently, specific humidity and θ_e further increase in the middle troposphere (Fig. 9e), which in return favors the convection activity. The pattern match between the specific humidity and θ_e indicates that the increased θ_e is primarily contributed by the increase of specific humidity then by the warming (Fig.9c). At the upper troposphere, forced by the latent heating, the warm-centered South Asian High strengthens over the IP (Fig. 9f), which is coupled with the cyclonic anomaly at low level (Fig. 9b), leading to moisture convergence over the western region and accelerate the convection activity. Positive feedback is thus built between precipitation and circulation. Regarding to HM uplift, there is not a circulation adjustment between the low and high levels, the precipitation-circulation coupling thus cannot be built.

In this thermodynamical process, the IP's blocking/mechanical effect is also noticeable as it blocks the cold dry extratropical airs from northern India where the airs of high θ_e cumulate (Fig. 9a). However, this effect is relatively weak given the small contribution of the easterly anomaly to precipitation increase (less than 0.3 mm day^{-1}, see Fig. 8a: $-< \mathrm{u}' \partial_x \overline{q} >$) according to the moisture budget.

https://doi.org/10.5194/cp-2024-8
Preprint. Discussion started: 26 February 2024

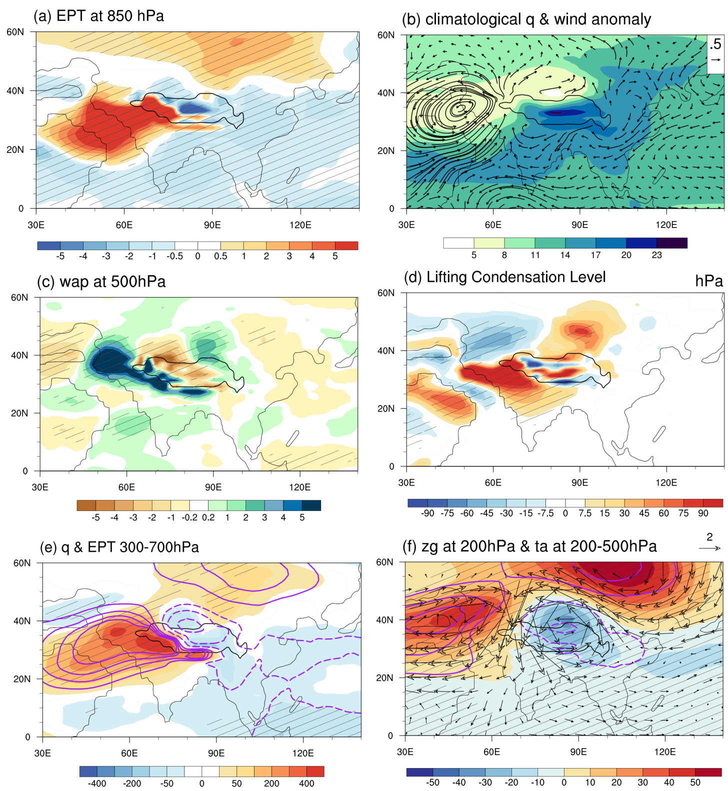

Figure 9. The differences of JJA mean thermal dynamical and dynamical variables between IP100HM100 and IP0HM0 simulations. (a) Equivalent Potential temperature (EPT, shading, unit: K) at 850 hPa; (b) climatological specific humidity q (shading, g/kg) and wind differences (vector, unit: m s^{-1}) at 850 hPa; (c) vertical velocity wap in pressure coordinate (-10^{-2} Pa/s) at 500 hPa; (d) Lifting condensation level (LCL, unit: hPa, positive value represent lower LCL); (e) Specific humidity (shading) and EPT (contours, unit: K) integrated between 300 and 700 hPa; (f) geopotential height zg (shading, unit: m), temperature anoamlies (contours, unit: K) and wind (vector, unit: m s^{-1}) at 200 hPa.

5. Discussion

5.1. Application to monsoonal reconstructions

A remarkable intensification of the SASM in the Middle Miocene is revealed by increasing evidence (Fig. 3c; Table 2). In the western India and the Arabian Sea, monsoon-like precipitation appeared in the early Miocene (Clift et al., 2008; Reuter et al., 2013; Ali et al., 2021) and intensified at ~15-12 Ma (Clift et al., 2008; Yang et al., 2020). In the eastern India, the intensification of SASM occurred at ca 15 Ma (Khan et al., 2014) to ~13-11 Ma (Bhatia et al., 2021; Vogali et al., 2017). In terms of wind system, a weaker "proto-monsoon" existed between 25 and 12.9 Ma (Betzler et al., 2016) and an abrupt intensification occurred at 12.9 Ma inferred from the sedimentary records in the Maldives (Betzler et al., 2016) and in the western Arabian Sea (Gupta et al., 2015), indicating the inception of a modern Somali Jet. Besides, monsoonal upwelling thus possibly the strengthening of wind speed in the western Arabian Sea was observed since ca 14.8 Ma and a major enhancement in the period 11-10 Ma (Zhuang et al., 2017).

Our modeling results support the existence of the SASM (Clift et al., 2008) in terms of precipitation seasonality in early Miocene represented by the IP0HM0 experiment when the proto-TP existed while the IP and HM were low (Fig.3). With the uplift of the IP rather than the HM during middle Miocene, monsoonal precipitation increased in the northwest of the Indian landmass as shown in the ~IP50, ~HM50 and IP100HM100 experiments (Fig.6) corroborating the hypothesis that increased sedimentary and weathering fluxes between 25 and 15 Ma could be partially linked with monsoon intensification related to the coeval of IP-HM (Clift et al., 2008). Meanwhile, with the deepening of cyclonical anomaly over the west of the IP (Fig.4b), southwesterly strengthens in the western Arabian Sea, which somewhat agrees with the reconstructions that suggests the inception of modern Somali Jet (Betzler et al., 2016; Zhuang et al., 2017). But the inception of modern Somali Jet is more likely attributed to the uplift of the East African topography (Chakraborty et al., 2006; Wei and Bondoni, 2016; Sarr et al., 2022; Tardif et al., 2023) and the emergence of land in Eastern Arabian Peninsula (Sarr et al., 2022). We conduct a series of complementary experiments (SM3) and confirm that elevated East African highlands plays an essential role in producing the modern-like Somali Jet. Meanwhile, it creates an anti-cyclonic anomaly over the north Arabian Sea as revealed previous studies, leading to reduced moisture transport into Indian landmass thus decreased monsoonal precipitation. Therefore, there is likely a complementary and competing effect on SASM evolution bewteen the uplift of the IP and the East African highlands.

The enhanced precipitation at 13 Ma is inferred from leaf fossil in the eastern HM, which has been attributed to the rise of the HM (Khan et al., 2014; Bhatia et al., 2021). But this hypothesis cannot be supported by our sensitivity experiment. Neither can it be interpreted by the uplift of the IP based on our simulations. In contrast, some modeling studies suggested enhanced precipitation in along the HM in response to mountain uplift in the American region and northern TP (Chakraborty et al., 2006; Miao et al., 2022). Therefore, remote impacts on precipitation change in the eastern HM should be taken into account.

The CO_2 forcing has little impact on the intensity of the Somali Jet, indicating its little contribution to the strengthening of surface wind inferred from the reconstructions (Gupta et al., 2015), but its effect on precipitation is likely to superimpose on that of the IP uplift. It is speculated that during the early part of the Middle Miocene Climatic Optimum, abrupt rise of the pCO_2 amplifies the effect of the IP uplift, leading to the markedly intensified SASM precipitation around 15 Ma as depicted in reconstructions (Clift et al., 2008; Yang et al., 2020). While during the mid-late Miocene, the decreasing tendency of pCO_2 offsets the effect of the IP uplift, although precipitation still intensifies due to the dominant impact of the latter. Given the wide range of reconstructed pCO_2 in terms of intensity and timing during the Middle Miocene, the effect of pCO_2 forcing experiences large uncertainty. Nevertheless, the CO2 variation itself cannot interpret the strengthening of wind along the Somali or the evolution of SASM precipitation intensity as inferred from the reconstructions.

5.2. Comparison with previous modeling studies

Concerning the effect of uplifted HM and IP on the SASM, our modeling results confirm the intensified SASM linked with the uplift of the IP (Liu et al., 2017; Zhang et al., 2015; Acosta and Huber, 2020; Tardif et al., 2020, 2023) rather than the HM (Zhang et al., 2012), particularly over the western region, i.e., from the Arabian Sea to the northwestern India and Pakistan. When the evolution history of the HM-TP is taken into account, the uplift of the HM against the TP mainly enhances the orographic precipitation along the windward side of the HM and has little impact on regional monsoonal precipitation.

Concerning the mechanism of the IP uplift on the SASM, our analyses tend to support its thermal forcing effect (Wu et al., 2012; Liu et al., 2017), but instead of emphasizing the sensible heating effect, we highlight the latent heating as a crucial link between the convection activity and regional circulations as previous study (He, 2017). This demonstrates that it is not only temperature, but also the hydrological cycle modifications as depicted in section 4 must be taken into account to understand the involved physical process. We also note that the IP's blocking/mechanical effect is much weaker in our study than that reported in Tang et al. (2013). In their study, the elevated IP effectively blocked the westerly flow to the south of the HM, facilitating the moisture advection from the Bay of Bengal into northern India, thus strongly enhanced the SASM precipitation, particularly in eastern India. Similar blocking effect (or role of gatekeeper) is also reported by Acosta and Huber (2020). The weak blocking effect in our study is likely due to: (1) smaller size of the IP in the Miocene than in the present day; (2) spatial lower-resolution model than that used in their studies (~1° or higher), thus some critical regional circulations linked to the SASM are likely misrepresented (Boos and Hurley, 2013; Acosta and Huber, 2017).

5.3. Uncertainty and Methodological Limitation

Geography is another important driver for Asian monsoon development (Ramstein et al., 1997; Farnsworth et al., 2019; Sarr et al., 2022; Tardif et al., 2023). The land-sea distribution used in our Miocene simulations reflects the feature of early to middle Miocene geography, in which the Tethyan Seaway is open, and the size of the IP is small. In the mid-late Miocene, given the final closure of the Tethyan Seaway ~14 Ma (Sun et al., 2021) and remarkable expansion of the Antarctic ice sheets from ~14.2 to 13.8 Ma (Frigola et al., 2018) leading to global sea-level change, the physiography in the Middle East and East Africa, a critical region for SASM development, is much different. As a result, the atmospheric and oceanic circulations are also changed in this region and far end (Hamon et al., 2013). But some modelling studies indicated that "the sole effect of the Tethys way closure, without strong modification of land extension in the Arabian Peninsula region, remain limited" (Tardif et al., 2023), in contrast to the hypothesis that the closure of the Tethys Seaway may contribute to altering the intensity of the monsoon during the Miocene (Bialik et al., 2020; Sun et al., 2021). Therefore, it is necessary in our future work to take into account of the effect of the paleogeography change, in particular the closure of the Tethys Seaway plus the development of the Anatolian Iranian Plateau. The evolution of the SASM during the Middle Miocene could have been caused by a combination of changes in topography，geography, the ocean-atmospheric circulation related to decreasing atmospheric CO_2, changes in orbital forcing, and the progressive cryosphere expansion on Antarctica. All these factors should be addressed in future study with careful experimental design.

High-resolution model is essential to capturing the monsoon dynamics and thermodynamics thus improves our understanding of the monsoonal variation/change (Acosta and Huber, 2017; Anand et al., 2018; Botsyun et al., 2022a,b). The climate model employed in present study is a version of low spatial resolution, not sufficient to reproduce the regional features of the SASM. For instance, the Indo-Gangetic low-level jet, a key mechanism that introduces monsoon onshore flow from the Bay of Bangla into northern India (Acosta and

https://doi.org/10.5194/cp-2024-8
Preprint. Discussion started: 26 February 2024

Huber, 2017), is missing in our modern simulation as all the low-resolution models do. Misrepresentation of this circulation is problematic for interpreting the effect of HM uplift and reconciling the modeling-proxy data discrepancy (Khan et al., 2014; Vogeli et al., 2017; Bhatia et al., 2021). The low resolution also likely underestimates the barrier effect of the IP due to topography smooth (Boos and Hurley, 2013). For instance, the mechanical blocking effect is more prominent in the studies with high-resolution models (Tang et al., 2013; Acosta and Huber, 2020) than those with coarse resolution model (Zhang et al., 2017; Wu et al., 2007). Although it is out of computer resources to run coupled paleoclimate simulations and perform many sensitivity experiments with high resolution version, we acknowledge that a better understanding of the impact of topographic change on the SASM and the underlying mechanism would benefit from additional simulations performed with increased spatial resolution.

The evolution of the SASM is also largely determined by large scale circulation (Wu et. al., 2012; Botsyun et al., 2022b). For instance, the mid-latitude westerly Jet migrated earlier (in the year) and reached higher latitude during warm climate periods than in the pre-industry (Botsyun et al., 2022b). Our Miocene experiments likely confirm this point (not shown) but investigation in depth needs to be done in the future.

6. Conclusions

In this study, we perform a series of 12 experiments with the fully couple OAGCM CESM1.2 (at ~2° horizontal resolution) to investigate how the SASM in response to topographic changes in the region surrounding the Tibetan Plateau and the variation of global CO_2 concentration during the Middle Miocene. On the one hand, we examine the effect of elevated IP and HM on the SASM with a set of topographic sensitivity experiments. On the other hand, due to the large uncertainties of CO_2 reconstructions (Rae et al., 2021; CenCO_2PIP, 2023), we provide a set of CO_2 sensitivity experiments to investigate its effect on the SASM. We explore the underlying mechanisms and compare the modeling results with proxy data. The conclusions are as follows:

(1) We confirm and extend previous studies that the IP uplift plays a major role in the intensification of the SASM, particularly in the western region, i.e., from the northern Arabian Sea to northwestern India and Pakistan, whereas it has little impact in eastern India. The effect of the HM uplift is confined to the range of the HM and its vicinity, producing orographic precipitation change.

https://doi.org/10.5194/cp-2024-8
Preprint. Discussion started: 26 February 2024

Climate of the Past
Discussions

(2) The SASM response to pCO_2 variation under the Middle Miocene boundary conditions is similar to that in present-day projecting future SASM change, suggesting similar physical process operating in the two warm periods. The enhanced monsoonal precipitation is primarily governed by enhanced thermodynamic conditions due to atmospheric warming, while the contribution from the change in large-scale monsoon circulation plays a secondary role. In the western part, topographic change, particular the IP uplift, still plays a dominant role.

(3) Topographic change out-competes CO_2 variation in driving the intensification of the SASM. The forcing of CO_2 variation is more important for the change of large-scale monsoon circulation that is decoupled with rainfall change. In the case of strong CO_2 variation, that is, from 280 to 1000 ppm, similar to the abrupt-3x or 4x CO_2 experiment), its contribution to SASM precipitation is comparable (ca 75%~100%) to that of topographic forcing in the core SAM region, but in the western region, topographical forcing is still the dominant factor.

(4) A thermodynamical process is proposed to link the uplift of the IP and enhanced SASM, in which deepened thermal low transporting moisture from the Arabian Sea to the western region is coupled with South Asian High linked by latent heating release. However, the strong thermal effect of uplifted IP in our Middle Miocene simulation is possibly linked to the smaller size of the IP as well as model's low-resolution that tends to underestimate the mechanical effect.

(5) Compared with reconstructions, the effect of IP uplift is in good agreement with observed evolution of precipitation and the change of wind intensity while the effects of the HM uplift and pCO_2 variation are inadequate to interpret the proxies.

Author contribution

MZ and YZ wrote the draft manuscript and analyzed the simulations. YS performed the simulations; GR and TZ modified the draft and particularly corrected the abstract and conclusions. YZ and DL conceived and developed the research. All authors participated in the final version of the manuscript.

Competing interest

The authors declare that they have no conflict of interest.

Acknowledgements

This work is jointly supported by the National Natural Science Foundation of China (Grants 41988101, 42105047) and the Second Tibetan Plateau Scientific Expedition and Research Program (STEP; Grant No. 2019QZKK0708). Model simulations presented in this study were performed on the supercomputer of Chinese Academy of Science Jin Cloud.

References

Acosta, R. P., and M. Huber, 2017: The neglected Indo-Gangetic plains low-level jet and its importance for moisture transport and precipitation during the peak summer monsoon. Geophysical Research Letters, 44, 8601-8610, https://doi.org/10.1002/2017gl074440.

Acosta, R.P., Huber, M., 2020. Competing Topographic Mechanisms for the Summer Indo-Asian Monsoon. Geophysical Research Letters 47, e2019GL085112. https://doi.org/10.1029/2019GL085112

Ali, S., E. C. Hathorne, and M. Frank, 2021: Persistent provenance of south asian monsoon-induced silicate weathering over the past 27 million years. Paleoceanography and Paleoclimatology, 36, https://doi.org/10.1029/2020pa003909.

Anand, A., Mishra, S.K., Sahany, S., Bhowmick, M., Rawat, J.S., Dash, S.K., 2018. Indian Summer Monsoon Simulations: Usefulness of Increasing Horizontal Resolution, Manual Tuning, and Semi-Automatic Tuning in Reducing Present-Day Model Biases. Sci Rep 8, 3522. https://doi.org/10.1038/s41598-018-21865-1

An, Z. S., J. E. Kutzbach, W. L. Prell, and S. C. Porter, 2001: Evolution of asian monsoons and phased uplift of the himalayan tibetan plateau since late miocene times. Nature, 411, 62-66, https://doi.org/10.1038/35075035.

Ballato, P., Cifelli, F., Heidarzadeh, G., Ghassemi, M.R., Wickert, A.D., Hassanzadeh, J., Dupont-Nivet, G., Balling, P., Sudo, M., Zeilinger, G., Schmitt, A.K., Mattei, M., Strecker, M.R., 2017. Tectono-sedimentary evolution of the northern Iranian Plateau: insights from middle–late Miocene foreland-basin deposits. Basin Research 29, 417–446. https://doi.org/10.1111/bre.12180

Betzler, C., and Coauthors, 2016: The abrupt onset of the modern south asian monsoon winds. Sci. Rep., 6, https://doi.org/10.1038/srep29838.

Bhatia, H., Srivastava, G., Spicer, R.A., Farnsworth, A., Spicer, T.E.V., Mehrotra, R.C., Paudayal, K.N., Valdes, P., 2021. Leaf physiognomy records the Miocene intensification of the South Asia Monsoon. Global and Planetary Change 196, 103365. https://doi.org/10.1016/j.gloplacha.2020.103365

Bialik, O. M., G. Auer, N. O. Ogawa, D. Kroon, N. D. Waldmann, and N. Ohkouchi, 2020: Monsoons, upwelling, and the deoxygenation of the northwestern indian ocean in response to middle to late miocene global climatic shifts. Paleoceanography and Paleoclimatology, 35, https://doi.org/10.1029/2019pa003762.

Boos, W., Kuang, Z., 2010. Dominant control of the South Asian Monsoon by orographic insulation versus plateau heating. Nature 463, 218–22. https://doi.org/10.1038/nature08707

Boos, W.R., Hurley, J.V., 2013. Thermodynamic Bias in the Multimodel Mean Boreal Summer Monsoon. Journal of Climate 26, 2279–2287. https://doi.org/10.1175/JCLI-D-12-00493.1

Botsyun, S., Ehlers, T.A., Koptev, A., Böhme, M., Methner, K., Risi, C., Stepanek, C., Mutz, S.G., Werner, M., Boateng, D., Mulch, A., 2022a. Middle Miocene Climate and Stable Oxygen Isotopes in Europe Based on Numerical Modeling. Paleoceanography and Paleoclimatology 37, e2022PA004442. https://doi.org/10.1029/2022PA004442

https://doi.org/10.5194/cp-2024-8
Preprint. Discussion started: 26 February 2024

Botsyun, S., Mutz, S.G., Ehlers, T.A., Koptev, A., Wang, X., Schmidt, B., Appel, E., Scherer, D.E., 2022b. Influence of Large-Scale Atmospheric Dynamics on Precipitation Seasonality of the Tibetan Plateau and Central Asia in Cold and Warm Climates During the Late Cenozoic. Journal of Geophysical Research: Atmospheres 127, e2021JD035810. https://doi.org/10.1029/2021JD035810

Burls, N.J., Bradshaw, C.D., Boer, A.M.D., Herold, N., Huber, M., Pound, M., Donnadieu, Y., Farnsworth, A., Frigola, A., Gasson, E., Heydt, A.S. von der, Hutchinson, D.K., Knorr, G., Lawrence, K.T., Lear, C.H., Li, X., Lohmann, G., Lunt, D.J., Marzocchi, A., Prange, M., Riihimaki, C.A., Sarr, A.-C., Siler, N., Zhang, Z., 2021. Simulating Miocene Warmth: Insights From an Opportunistic Multi-Model Ensemble (MioMIP1). Paleoceanography and Paleoclimatology 36, e2020PA004054. https://doi.org/10.1029/2020PA004054

Chakraborty, A., Nanjundiah, R.S., Srinivasan, J., 2006. Theoretical aspects of the onset of Indian summer monsoon from perturbed orography simulations in a GCM. Annales Geophysicae 24, 2075–2089.

Chen, G.-S., Liu, Z., Kutzbach, J., 2014. Reexamining the barrier effect of the Tibetan Plateau on the South Asian summer monsoon. Climate of the Past 10. https://doi.org/10.5194/cp-10-1269-2014

Chou, C., J. D. Neelin, C.-A. Chen, and J.-Y. Tu, 2009: Evaluating the "rich-get-richer" mechanism in tropical precipitation change under global warming. J. Climate, 22, 1982-2005, https://doi.org/10.1175/2008jcli2471.1.

Clift, P.D., Hodges, K.V., Heslop, D., Hannigan, R., Van Long, H., Calves, G., 2008. Correlation of Himalayan exhumation rates and Asian monsoon intensity. Nature Geosci 1, 875–880. https://doi.org/10.1038/ngeo351

Clift, P.D., Webb, A.A.G., 2019. A history of the Asian monsoon and its interactions with solid Earth tectonics in Cenozoic South Asia. Geological Society, London, Special Publications 483, 631–652. https://doi.org/10.1144/SP483.1

Ding, L., Spicer, R.A., Yang, J., Xu, Q., Cai, F., Li, S., Lai, Q., Wang, H., Spicer, T.E.V., Yue, Y., Shukla, A., Srivastava, G., Khan, M.A., Bera, S., Mehrotra, R., 2017. Quantifying the rise of the Himalaya orogen and implications for the South Asian monsoon. Geology 45, 215–218. https://doi.org/10.1130/G38583.1

Ding, L., P. Kapp, F. Cai, C. N. Garzione, Z. Xiong, H. Wang, and C. Wang, 2022: Timing and mechanisms of tibetan plateau uplift. Nature Reviews Earth & Environment, https://doi.org/10.1038/s43017-022-00318-4.

Endo, H., and A. Kitoh, 2014: Thermodynamic and dynamic effects on regional monsoon rainfall changes in a warmer climate. Geophysical Research Letters, 41, 1704-1710, https://doi.org/10.1002/2013gl059158.

Eyring, V., Bony, S., Meehl, G.A., Senior, C.A., Stevens, B., Stouffer, R.J., Taylor, K.E., 2016. Overview of the Coupled Model Intercomparison Project Phase 6 (CMIP6) experimental design and organization. Geoscientific Model Development 9, 1937–1958. https://doi.org/10.5194/gmd-9-1937-2016

Farnsworth, A., Lunt, D.J., Robinson, S.A., Valdes, P.J., Roberts, W.H.G., Clift, P.D., Markwick, P., Su, T., Wrobel, N., Bragg, F., Kelland, S.-J., Pancost, R.D., 2019. Past East Asian monsoon evolution controlled by paleogeography, not CO2. Science Advances 5, eaax1697. https://doi.org/10.1126/sciadv.aax1697

Fluteau, F., Ramstein, G., Besse, J., 1999. Simulating the evolution of the Asian and African monsoons during the past 30 Myr using an atmospheric general circulation model. Journal of Geophysical Research: Atmospheres 104, 11995–12018. https://doi.org/10.1029/1999JD900048

Frigola, A., Prange, M., Schulz, M., 2018. Boundary conditions for the Middle Miocene Climate Transition (MMCT v1. 0). Geoscientific Model Development 11, 1607–1626.

https://doi.org/10.5194/cp-2024-8
Preprint. Discussion started: 26 February 2024

Gent, P.R., Danabasoglu, G., Donner, L.J., Holland, M.M., Hunke, E.C., Jayne, S.R., Lawrence, D.M., Neale, R.B., Rasch, P.J., Vertenstein, M., Worley, P.H., Yang, Z.-L., Zhang, M., 2011. The Community Climate System Model Version 4. Journal of Climate 24, 4973–4991. https://doi.org/10.1175/2011JCLI4083.1

Goldner, A., Herold, N., Huber, M., 2014. The Challenge of Simulating the Warmth of the Mid-Miocene Climatic Optimun in CESM1. Climate of the Past.

Gupta, A. K., A. Yuvaraja, M. Prakasam, S. C. Clemens, and A. Velu, 2015: Evolution of the south asian monsoon wind system since the late middle miocene. Palaeogeography Palaeoclimatology Palaeoecology, 438, 160-167, https://doi.org/10.1016/j.palaeo.2015.08.006.

Hamon, N., Sepulchre, P., Lefebvre, V., Ramstein, G., 2013. The role of eastern Tethys seaway closure in the Middle Miocene Climatic Transition (ca. 14 Ma). Climate of the Past 9, 2687–2702. https://doi.org/10.5194/cp-9-2687-2013

Harris, N., 2006. The elevation history of the Tibetan Plateau and its implications for the Asian monsoon. Palaeogeography, Palaeoclimatology, Palaeoecology, Monsoon and Tectonics of Asia 241, 4–15. https://doi.org/10.1016/j.palaeo.2006.07.009

He, B., 2017. Influences of elevated heating effect by the Himalaya on the changes in Asian summer monsoon. Theor Appl Climatol 128, 905–917. https://doi.org/10.1007/s00704-016-1746-5

Herold, N., M. Huber, and R. D. Mueller, 2011: Modeling the miocene climatic optimum. Part i: Land and atmosphere. J. Climate, 24, 6353-6372, https://doi.org/10.1175/2011jcli4035.1.

Hersbach, H., and Coauthors, 2020: The era5 global reanalysis. Quarterly Journal of the Royal Meteorological Society, 146, 1999-2049, https://doi.org/10.1002/qj.3803.

Huffman, G. J., R. F. Adler, D. T. Bolvin, and G. Gu, 2009: Improving the global precipitation record: Gpcp version 2.1. Geophys. Res. Lett., 36, https://doi.org/10.1029/2009gl040000.

Hunke, E.C., Lipscomb, W.H., 2010. CICE: the Los Alamos Sea Ice Model Documentation and Software User's Manual Version 4. 1–76.

Jin, C., B. Wang, and J. Liu, 2020: Future changes and controlling factors of the eight regional monsoons projected by cmip6 models. J. Climate, 33, 9307-9326, https://doi.org/10.1175/jcli-d-20-0236.1.

Khan, M.A., Spicer, R.A., Bera, S., Ghosh, R., Yang, J., Spicer, T.E.V., Guo, S., Su, T., Jacques, F., Grote, P.J., 2014. Miocene to Pleistocene floras and climate of the Eastern Himalayan Siwaliks, and new palaeoelevation estimates for the Namling–Oiyug Basin, Tibet. Global and Planetary Change 113, 1–10. https://doi.org/10.1016/j.gloplacha.2013.12.003

Kitoh, A., 2002. Effects of Large-Scale Mountains on Surface Climate. A Coupled Ocean-Atmosphere General Circulation Model Study. Journal of the Meteorological Society of Japan 80, 1165–1181. https://doi.org/10.2151/jmsj.80.1165

Kong, Y., Y. Wu, X. Hu, Y. Li, and S. Yang, 2022: Uncertainty in projections of the south Asian summer monsoon under global warming by cmip6 models: Role of tropospheric meridional thermal contrast. Atmospheric and Oceanic Science Letters, 15, 100145, https://doi.org/https://doi.org/10.1016/j.aosl.2021.100145.

Krapp, M., and J. H. Jungclaus, 2011: The middle miocene climate as modelled in an atmosphere-ocean-biosphere model. Climate Past, 7, 1169-1188, https://doi.org/10.5194/cp-7-1169-2011.

Kutzbach, J.E., Guetter, P.J., Ruddiman, W.F., Prell, W.L., 1989. Sensitivity of climate to late Cenozoic uplift in southern Asia and the American west: Numerical experiments. Journal of Geophysical Research: Atmospheres 94, 18393–18407. https://doi.org/10.1029/JD094iD15p18393

Lawrence, D.M., Oleson, K.W., Flanner, M.G., Thornton, P.E., Swenson, S.C., Lawrence, P.J., Zeng, X., Yang, Z.-L., Levis, S., Sakaguchi, K., Bonan, G.B., Slater, A.G., 2011.

https://doi.org/10.5194/cp-2024-8
Preprint. Discussion started: 26 February 2024

Climate of the Past
Discussions

Parameterization improvements and functional and structural advances in Version 4 of the Community Land Model. Journal of Advances in Modeling Earth Systems 3, M03001. https://doi.org/10.1029/2011MS00045

Licht, A., and Coauthors, 2014: Asian monsoons in a late eocene greenhouse world. Nature, 513, 501-506, https://doi.org/10.1038/nature13704.

Liu, X., and B. Dong, 2013: Influence of the tibetan plateau uplift on the asian monsoon-arid environment evolution. Chinese Science Bulletin, 58, 4277-4291, https://doi.org/10.1007/s11434-013-5987-8.

Liu, X., Xu, Q., Ding, L., 2016. Differential surface uplift: Cenozoic paleoelevation history of the Tibetan Plateau. Sci. China Earth Sci. 59, 2105–2120. https://doi.org/10.1007/s11430-015-5486-y

Liu, Y., Wang, Z., Zhuo, H., Wu, G., 2017. Two types of summertime heating over Asian large-scale orography and excitation of potential-vorticity forcing II. Sensible heating over Tibetan-Iranian Plateau. Sci. China Earth Sci. 60, 733–744. https://doi.org/10.1007/s11430-016-9016-3

Manabe, S., Terpstra, T.B., 1974. The Effects of Mountains on the General Circulation of the Atmosphere as Identified by Numerical Experiments. Journal of the Atmospheric Sciences 31, 3–42. https://doi.org/10.1175/1520-0469(1974)031<0003:TEOMOT>2.0.CO;2

McQuarrie, N., Stock, J.M., Verdel, C., Wernicke, B.P., 2003. Cenozoic evolution of Neotethys and implications for the causes of plate motions. Geophysical Research Letters 30. https://doi.org/10.1029/2003GL017992

Mouthereau, F., 2011. Timing of uplift in the Zagros belt/Iranian plateau and accommodation of late Cenozoic Arabia–Eurasia convergence. Geological Magazine 148, 726–738. https://doi.org/10.1017/S0016756811000306

Neale, R.B., Richter, J., Park, S., Lauritzen, P.H., Vavrus, S.J., Rasch, P.J., Zhang, M., 2013. The Mean Climate of the Community Atmosphere Model (CAM4) in Forced SST and Fully Coupled Experiments. Journal of Climate 26, 5150–5168. https://doi.org/10.1175/JCLI-D-12-00236.1

Prell, W. L., and J. E. Kutzbach, 1992: Sensitivity of the indian monsoon to forcing parameters and implications for its evolution. Nature, 360, 647-652, https://doi.org/10.1038/360647a0.

Ramstein, G., Fluteau, F., Besse, J., Joussaume, S., 1997. Effect of orogeny, plate motion and land-sea distribution on Eurasian climate change over the past 30 million years. Effect of orogeny, plate motion and land-sea distribution on Eurasian climate change over the past 30 million years 386, 788–795.

Reuter, M., W. E. Piller, M. Harzhauser, and A. Kroh, 2013: Cyclone trends constrain monsoon variability during late oligocene sea level highstands (kachchh basin, nw india). Climate Past, 9, 2101-2115, https://doi.org/10.5194/cp-9-2101-2013.

Sarr, A.-C., and Coauthors, 2022: Neogene south asian monsoon rainfall and wind histories diverged due to topographic effects. Nat Geosci, 15, 314-+, https://doi.org/10.1038/s41561-022-00919-0.

Smith, R., P. Jones, B. Briegleb, F. Bryan, and S. Yeager, 2010: The parallel ocean program (pop) reference manual: Ocean component of the community climate system model (ccsm).

Steinthorsdottir, M., Coxall, H., De Boer, A., Huber, M., Barbolini, N., Bradshaw, C., Burls, N., Feakins, S., Gasson, E., Henderiks, J., Holbourn, A.E., Kiel, S., Kohn, M., Knorr, G., Kürschner, W.M., Lear, C.H., Liebrand, D., Lunt, D.J., Mörs, T., Pearson, P., Pound, M.J., Stoll, H., Stromberg, C., 2021. The Miocene: The Future of the Past. Paleoceanography and Paleoclimatology 36. https://doi.org/10.1029/2020PA004037

Su, B., Jiang, D., Zhang, R., Sepulchre, P., Ramstein, G., 2018. Difference between the North Atlantic and Pacific meridional overturning circulation in response to the uplift of the Tibetan Plateau. Climate of the Past 14, 751–762. https://doi.org/10.5194/cp-14-751-2018

Sun, J., Sheykh, M., Ahmadi, N., Cao, M., Zhang, Z., Tian, S., Sha, J., Jian, Z., Windley, B.F., Talebian, M., 2021. Permanent closure of the Tethyan Seaway in the northwestern Iranian Plateau driven by cyclic sea-level fluctuations in the late Middle Miocene. Palaeogeography, Palaeoclimatology, Palaeoecology 564, 110172. https://doi.org/10.1016/j.palaeo.2020.110172

Sun, Y., and Coauthors, 2023: Revisiting the physical mechanisms of east Asian summer monsoon precipitation changes during the mid-Holocene: A data–model comparison. Climate Dynamics, 60, 1009-1022, https://doi.org/10.1007/s00382-022-06359-1.

Tada, R., H. Zheng, and P. D. Clift, 2016: Evolution and variability of the asian monsoon and its potential linkage with uplift of the himalaya and tibetan plateau. Progress in Earth and Planetary Science, 3, https://doi.org/10.1186/s40645-016-0080-y.

Tang, H., Micheels, A., Eronen, J.T., Ahrens, B., Fortelius, M., 2013. Asynchronous responses of East Asian and Indian summer monsoons to mountain uplift shown by regional climate modelling experiments. Clim Dyn 40, 1531–1549. https://doi.org/10.1007/s00382-012-1603-x

Tardif, D., Fluteau, F., Donnadieu, Y., Le Hir, G., Ladant, J.-B., Sepulchre, P., Licht, A., Poblete, F., Dupont-Nivet, G., 2020. The origin of Asian monsoons: a modelling perspective. Climate of the Past 16, 847–865. https://doi.org/10.5194/cp-16-847-2020

Tardif, D., and Coauthors, 2023: The role of paleogeography in Asian monsoon evolution: A review and new insights from climate modelling. Earth-Science Reviews, 243, 104464, https://doi.org/https://doi.org/10.1016/j.earscirev.2023.104464.

The Cenozoic, C. O. P. I. P. C., and Coauthors: Toward a Cenozoic history of atmospheric co2. Science, 382, eadi5177, https://doi.org/10.1126/science.adi5177.

Vogeli, N., P. Huyghe, P. van der Beek, Y. Najman, E. Garzanti, and C. Chauvel, 2017: Weathering regimein the eastern himalaya since the mid-miocene: Indications fromdetrital geochemistry and claymineralogy of the kameng river section, arunachal pradesh, india. Basin Research, 30, 59-74, https://doi.org/10.1111/bre.12242.

Wang, C., Dai, J., Zhao, X., Li, Y., Graham, S.A., He, D., Ran, B., Meng, J., 2014. Outward-growth of the Tibetan Plateau during the Cenozoic: A review. Tectonophysics 621, 1–43. https://doi.org/10.1016/j.tecto.2014.01.036

Wang, Z., Duan, A., Yang, S., 2019. Potential regulation on the climatic effect of Tibetan Plateau heating by tropical air–sea coupling in regional models. Clim Dyn 52, 1685–1694. https://doi.org/10.1007/s00382-018-4218-z

Wu, G., Liu, Y., He, B., Bao, Q., Duan, A., Jin, F.-F., 2012. Thermal Controls on the Asian Summer Monsoon. Scientific Reports 2, 404. https://doi.org/10.1038/srep00404

Wu, G., Liu, Y., Zhang, Q., Duan, A., Wang, T., Wan, R., Liu, X., Li, W., Wang, Z., Liang, X., 2007. The Influence of Mechanical and Thermal Forcing by the Tibetan Plateau on Asian Climate. Journal of Hydrometeorology 8, 770–789. https://doi.org/10.1175/JHM609.1

Yang, X., Groeneveld, J., Jian, Z., Steinke, S., Giosan, L., 2020. Middle Miocene Intensification of South Asian Monsoonal Rainfall. Paleoceanography and Paleoclimatology 35, e2020PA003853. https://doi.org/10.1029/2020PA003853

Zhang, R., Jiang, D., Liu, X., Tian, Z., 2012. Modeling the climate effects of different subregional uplifts within the Himalaya-Tibetan Plateau on Asian summer monsoon evolution. Chin. Sci. Bull. 57, 4617–4626. https://doi.org/10.1007/s11434-012-5284-y

Zhang, R., Jiang, D., Zhang, Z., 2019. Vegetation and Ocean Feedbacks on the Asian Climate Response to the Uplift of the Tibetan Plateau. Journal of Geophysical Research: Atmospheres 124, 6327–6341. https://doi.org/10.1029/2019JD030503

Zhang, R., Jiang, D., Zhang, Z., Yu, E., 2015. The impact of regional uplift of the Tibetan Plateau on the Asian monsoon climate. Palaeogeography, Palaeoclimatology, Palaeoecology 417, 137–150. https://doi.org/10.1016/j.palaeo.2014.10.030

https://doi.org/10.5194/cp-2024-8
Preprint. Discussion started: 26 February 2024

Zhuang, G., Pagani, M., Zhang, Y.G., 2017. Monsoonal upwelling in the western Arabian Sea since the middle Miocene. Geology 45, 655–658. https://doi.org/10.1130/G39013.1

https://doi.org/10.5194/cp-2024-8
Preprint. Discussion started: 26 February 2024

Table 1. Simulations performed with CESM1.2 in this study. See Fig.2 for modern and paleogeography maps.

experiment	Geolography	vegetation	pCO2 (ppm)	IP	HM
piControl	Modern	Modern	280	Modern	Modern
MMIO (IP100HM80)	M.Miocene*	M.Miocene	400	M.Miocene	M.Miocene
IP0HM0	M.Miocene	M.Miocene	400	0	0
IP50HM0	M.Miocene	M.Miocene	400	50%	0
IP100HM0	M.Miocene	M. Miocene	400	100%	0
IP0HM100	M.Miocene	M.Miocene	400	0	100%**
IP50HM100	M.Miocene	M.Miocene	400	50%	100%
IP100HM100	M. Miocene	M. Miocene	400	100%	100%
MMIO280	M. Miocene	M.Miocene	280	M. Miocene	M.Miocene
MMIO1000	M.Miocene	M.Miocene	1000	M. Miocene	M.Miocene

*M.Miocen: Middle Miocene

** 100% of the height of modern HM.

https://doi.org/10.5194/cp-2024-8
Preprint. Discussion started: 26 February 2024

850 **Table 2.** Evidences of modern SAM in middle Miocene from recently published studies.

No	station	Location (lat/lon)	sample	Intensification age (Ma)	Trend*	variable	references
1	Well Indus Marine A-1	24/66	weathering	15~12	decreasing	Precip	Clift et al., 2008
2	ODP 359	5/73	deposit	12.9	increasing	wind	Betzler et al., 2016
3	ODP 722B	16.6/59.8	Bio-marker	12.9	increasing	wind	Gupta et al., 2015
	ODP 722B	16.6/59.8	Bio-marker	11	increasing	wind	Zhuang et al., 2017
	ODP 722B	16.6/59.8	Bio-marker	14	increasing	Precip	Bialik et al., 2020
4	NGHP-01-01A	15/71	Bio-marker	14	increasing	Precip	Yang et al., 2020
5	Varkala	8.7/76.7	Pollen fossil	17-15	No change	Precip.	Reuter et al., 2013
6	ODP 758	5.4/90.4	weathering	13.9	increasing	Precip	Ali et al., 2021
7	Surai Khola	27.8/83	Leaf Fossil	13	increasing	Precip.	Srivastava et al., 2018 Bhatia et al., 2021
8	Darjeeling	27/88.5	Leaf Fossil	13	increasing	Precip.	Khan et al., 2014
9	Arunachal Pradesh	27/93.5	Leaf Fossil	13	No change	Precip.	Khan et al., 2014
	Arunachal Pradesh	26/93.5	weathering	13	No change	Precip.	Vogeli et al., 2017

851 * Trend of monsoon index change from middle to late Miocene.
852